60 GHz Low-Noise Amplifier in a 70 nm GaAs m-HEMT Technology

for Multi-band Impulse Detection System

Pape Sanoussy Diao, Thierry Alves, Benoît Poussot and Martine Villegas

Université Paris-Est, ESYCOM (FRE2028), CNAM, CNRS, ESIEE Paris, Université Paris-Est Marne-la-Vallée
F-77454 Marne-la-Vallée, France
Email: `pape-sanoussy.diao@esiee.fr`, `thierry.alves@esiee.fr`

Abstract—**In this paper, we present a 60 GHz Low-Noise Amplifier (LNA) to improve the performance of multi-band detection systems. The LNA is designed in 70 nm GaAs metamorphic High Electron Mobility Transistor (m-HEMT) technology and occupies an area of 1.47 x 1.0 mm^2. The inductive degeneration technique is used for a suitable trade-off between gain and noise. The three-stage LNA achieves a gain of 14.3 dB and a noise factor of 2.1 dB at 60.2 GHz, while consuming 13.5 mW. The simulated non-linear characteristics show an IP_{1dB} (Input 1 dB compression Point) of -9.6 dBm and an $IIP3$ (Input third-order Intercept Point) of -4.8 dBm.**

Keywords–LNA; 60 GHz; GaAs m-HEMT; Millimeter wave technology; Multi-band detection system.

I. INTRODUCTION

Advances in integrated circuit technologies are generating great interest in the evolution of standards in millimeter-wave bands. The availability of unlicensed bandwidth around 60 GHz in several regions of the world (57-66 GHz in Europe) is a real opportunity for new systems development and frequency harmonisation. Advances in SiGe [1] [2] and III-V [3]- [5] technologies nowadays allow the production of devices and systems for a variety of applications in millimeter-wave bands. These opportunities create a need for increasingly high-performance devices. In this way, this work adresses the design of a wideband amplifier, wich has low-noise, low power consumption and is small in size in order to improve the performance of detection systems.

This study is part of the development of an Ultra-WideBand (UWB) millimeter-wave detection system for short-range applications. We consider the monostatic radar context, Figure 1, with a cylindrical metallic target of radius r and height h $(r; h)$. The detection system is schematized by a transceiver (TX-RX) using the same antenna. The incidence angle θ is determined by the orientation of the target with respect to the antenna boresight.
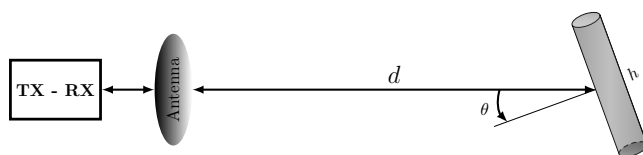

Figure 1. Context of the detection

This paper proposes the design of a low-noise amplifier with the 70 nm GaAs m-HEMT technology from OMMIC. It

is structured as follows: Section II presents the principle of detection. Section III presents the sizing of the system and LNA specifications. Choice and technology description are presented in Section IV. Then, the design of the circuit is detailed in Section V. In Section VI, we present the results of the post-layout electromagnetic simulations in comparison with those in the literature before concluding in Section VII.

II. PRINCIPLE OF DETECTION

The angular dependence of the Radar Cross Section (RCS) of objects often results in a limitation of the detection range when moving away from the normal incidence. To overcome this limitation, we use frequency diversity [6]. The proposed detection principle is then based on the impulse technique, using a multi-band approach [7] [8], to improve detection coverage, particularly the continuity of detection according to the target orientation angle θ. Frequencies around 60 GHz were chosen for spectrum availability, but also for short wavelengths (5 mm at 60 GHz) to detect small objects (< 10 cm). The architecture associated with the detection principle is shown in Figure 2 for a dual-band system at 57.8 GHz and 62.8 GHz. In the transmitter, Differential Structure Power Amplifiers (DSPAs) whose operation is based on the even mode rejection are used. DSPA$_1$ provides both signal division
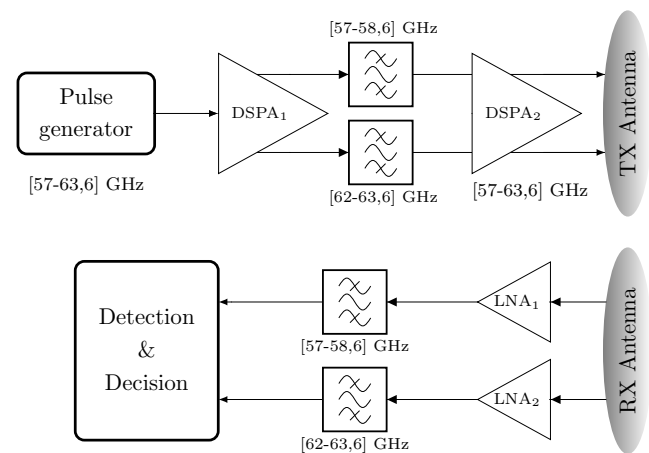

Figure 2. Dual-band detection architecture

and pre-amplification. The signals selected by the filter bank are then amplified by DSPA$_2$ and transmitted by the same antenna. In reception, simple LNAs are used for better noise

performance. The received signals are selected by a filter bank identical to the one in transmission before being subjected to the detection and decision process. More details of the architecture operation are given in [8]. This architecture can be applied in a more general case with N bands. The processing of the received signals can be done by different techniques, such as: selection combining, cumulative detection [8], or non-coherent integration [9].

III. System Sizing and LNA Specifications

The sizing of the system is based on the monostatic radar equation expressing the maximum detection range (R_{max}) as a function of the minimum detectable power S_{min} [10]:

$$R_{max}^4 = \frac{P_t G^2 \lambda^2 \sigma}{(4\pi)^3 S_{min}} \tag{1}$$

where P_t is the transmitted power, G is the antenna gain, λ the operating wavelength and σ the RCS of the target.

Since S_{min} is related to the thermal noise power of the receiver and the minimum Signal-to-Noise Ratio (SNR) required to detect a target, the radar equation (1) can be written in the form:

$$R_{max}^4 = \frac{P_t G^2 \lambda^2 \sigma}{(4\pi)^3 \cdot kT\Delta f \cdot F \cdot SNR_r} \tag{2}$$

where k is the Boltzmann constant, T the temperature, Δf the receiver bandwidth, F its noise factor and SNR_r the required SNR at the output of the receiver to ensure detection.

In the equation (2), the transmitted power and the antenna gain are determined by standardization. The wavelength λ is chosen according to the application and the dimensions of the targets to be detected. The receiver bandwidth Δf is defined by the bandwidth of the front-end filter which will set the range resolution ΔR of the system ($\Delta R = c/2\Delta f$). The SNR_r is defined by the desired performance in terms of detection and false alarm probabilities. The proposed detection principle is based on the frequency and angle variations of the RCS. Thus, the receiver noise factor F is the only adjustable parameter to maximize system performance. Due to the position of the LNA in the receiver architecture, shown in Figure 2, the impact of its noise factor is more significant over that of the total RF chain according to the Friis equation:

$$F = F_1 + \frac{F_2 - 1}{G_1} + \frac{F_3 - 1}{G_1 G_2} + ... + \frac{F_n - 1}{G_1 G_2 ... G_{n-1}} \tag{3}$$

where F_i and G_i are the noise factor and the power gain, respectively, of the i-th stage, and n is the number of stages. By setting the objective of detecting a cylindrical target ($r = 0.6$ cm; $h = 5.4$ cm), up to 2 m at normal incidence, we will determine the characteristics of the receiver stage and in particular those of the LNA. For this purpose, we consider a system with four bands in 57-66 GHz, distributed around the frequencies 57.8 GHz, 60.2 GHz, 62.8 GHz and 65.2 GHz. The output power of each channel of the $DSPA_2$ is set at 15 dBm (taking into account frequency bands standardization) and the gain of the antennas at 12 dBi (which can be achieved with 4 patches of 6 dBi each). The bandwidth of each band is 1.6 GHz and the SNR_r depends on the detection technique used. Filter losses are set at 3.5 dB [11]. For a conventional single-band configuration, the SNR_r to ensure the detection

of a nonfluctuating target with a detection probability of 90% and a false alarm probability of 10^{-6} is 13.2 dB [10]. In the case of a non-coherent integration of 4 pulses in 4 sufficiently spaced frequency bands, the SNR_r is only 8.3 dB for the same detection and false alarm probabilities. Based on this case of non-coherent integration, using (2), we established the technical specifications of the LNA given in Table I, to ensure the targeted detection.

TABLE I. TECHNICAL SPECIFICATIONS OF THE LNA

Parameters	Values
Bandwidth BW	≥ 1.6 GHz
Power gain G	≥ 12.5 dB
Noise factor NF	< 3 dB
S_{11} & S_{22}	< -10 dB

IV. Choice and Description of the Technology

To realize the LNA, we have two design technologies: SG13S from IHP (Innovations for High Performance) Micro-electronics [12] and D007IH from OMMIC [13]. The choice of technology was first based on a study of passive elements. This revealed that SG13S is better suited for highly integrable components (small capacitors and resistors). On the other hand, it has very high losses (≈ 0.7 dB/mm @ 60 GHz) for low-noise applications. Unlike SG13S, the D007IH has the advantage of lower losses (≈ 0.22 dB/mm @ 60 GHz) and more integrable inductors in terms of shape. For example, Figure 3 shows simulation results of grounded transmission lines of the same characteristic impedance of 75 Ω. It can be seen that the D007IH has a quality factor (Q-factor) more than 5 times higher than that of the SG13S at 60 GHz for the same inductance of 268 pH.
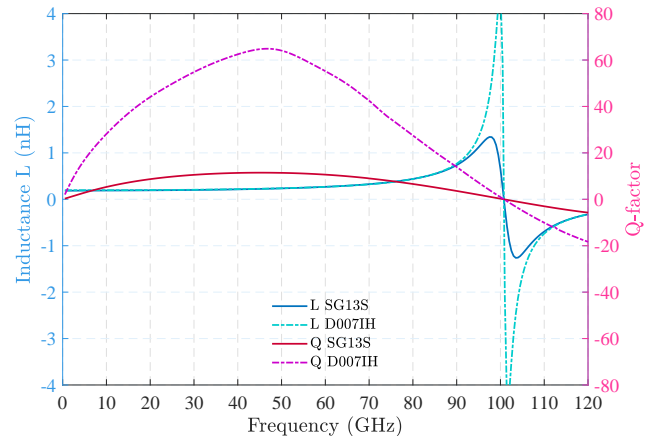

Figure 3. Comparison of grounded transmission lines

At high frequencies and especially at 60 GHz, the use of transmission lines is often preferred, so the D007IH seems more suitable for low noise applications. However, in microwaves, the overall performance of a circuit depends not only on the passive elements, but also on the characteristics of the transistors. Thus, the choice of technology must be based on an analysis of the global circuit. For this purpose, we compared single-stage amplifiers designed with both technologies, Table II. This comparison clearly shows that the m-HEMT is

TABLE II. SINGLE STAGE AMPLIFIERS COMPARISON

Technology	Transistor	Gain (dB)	NF (dB)	P_{DC} (mW)
SG13S	Bipolar	4.0	2.6	2.0
SG13S	MOS	3.1	2.6	9.2
D007IH	m-HEMT	3.9	1.2	4.1

the only one of the three transistor models that can meet the technical specifications of the LNA, particularly in terms of noise. To satisfy the gain performance, the use of a multi-stage structure will be necessary. In addition, with regard to sizing, it appeared that the noise factor is more significant over the gain because its influence is much greater in the range of the system. So, D007IH technology is chosen for the design of the LNA.

D007IH is a 70 nm gate length GaAs technology providing f_T/f_{max} of 300 GHz/450 GHz. It offers a depletion transistor m-HEMT with very high transconductance of $g_{m_{max}} = 1600$ mS/mm, that can support a voltage $V_{DS_{max}}$ of 3 V and a maximum current $I_{DSS_{max}}$ of 400 mA/μm. This type of transistor offers good performance in terms of noise, with a noise factor of only 0.5 dB at 30 GHz, giving it a privilege for security applications (millimeter-band imaging), telecommunications or radars. The process of the technology consists of a 3.5 μm metal in its underside, a 100 μm thick GaAs substrate above which different metallization levels can be distinguished. The most used metal layer for transmission lines realization is the IN metal with a thickness of 1.25 μm. It is also possible to associate this layer with a gold layer of the same thickness for less losses.

V. CIRCUIT DESIGN

The circuit is designed with Keysight Advanced Design System (ADS). The LNA consists of a three-stage structure using identical transistors. The size of the transistor is chosen so as to ensure a better trade-off between gain and noise. A parametric study allowed us to choose a transistor of 2 x 25 μm grid development. The optimal bias point then corresponds to a voltage $V_{DS} = 1$ V for an I_{DS} current of about 4.1 mA.

Unconditional stability has been ensured both by inductive degeneration of the source, but also by the use of a resistance in the bias circuit. This resistance allows stability at low frequency; its value must be chosen meticulously because it influences the gain and noise [14]. The degeneration also brings the circles of gain and noise closer together and thus facilitates the input matching [15].

The first two stages are almost identical and are matched with a good trade-off between gain and noise. Matching of the third stage is optimized in gain because its influence is less on the noise factor of the whole structure (3). The LNA's first stage schematic is presented in Figure 4.

The bias circuits are made with quarter-wave transmission lines. They include GaAs implanted resistors (R_D and R_G) for improving low frequency stability and by-pass capacitors (C_D) to short RF (Radio Frequency) leakage to the ground. The degeneration of the transistor source is ensured by the shorted transmission line TL_S. The capacitor C_1 and the transmission lines TL_1 and TL_2 form the input matching network. TL_1 is an open line smaller than $\lambda/4$ and therefore acts as a parallel capacitor. C_2, TL_3 and C_3 form the inter-stage matching and DC (Direct Current) isolation between stages 1 and 2. The

same topology is used between stages 2 and 3. The output matching of the LNA is performed by a simple L-C series topology. The output inductor is achieved by a transmission line whose dimensions are optimized for a better gain, without degrading the noise factor, while respecting the design rules.
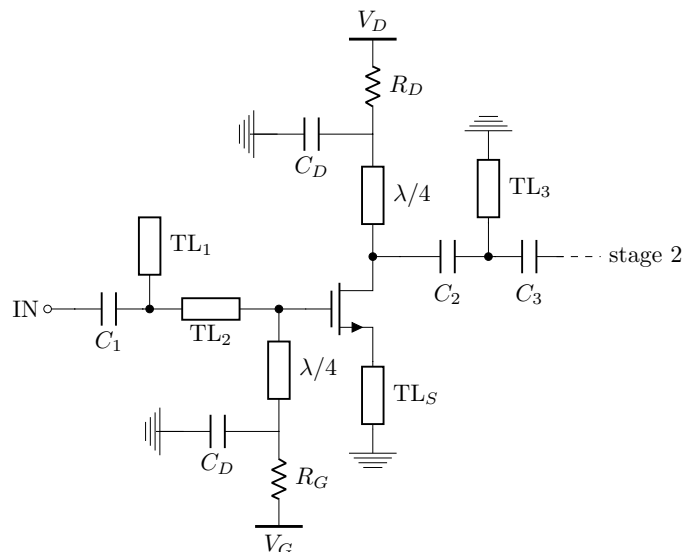
Figure 4. Schematic of the first stage of the LNA

VI. POST-LAYOUT SIMULATIONS RESULTS

The layout of the LNA is shown in Figure 5 and it includes RF and DC pads. All transmission lines are made with the same IN metal layer. Ground connections are made using vias holes. The size of the circuit is 1.47 x 1.0 mm^2.
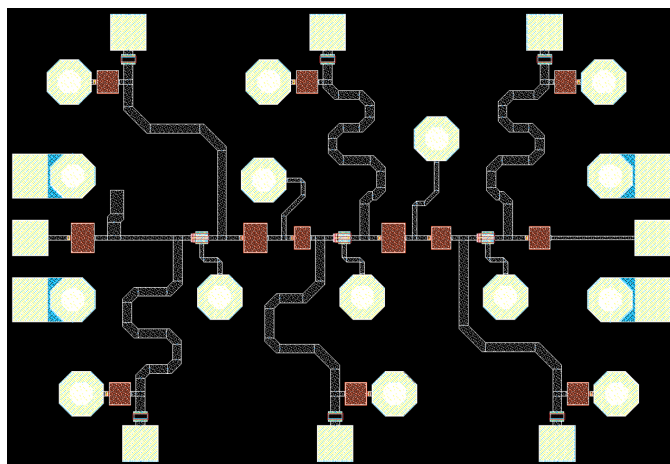
Figure 5. Layout of the LNA

For layout realization, small transmission lines have been added to transistor accesses (gate and drain) to reduce the coupling between components. The resistor in the drain bias drops the voltage at the DC pad from 1.1 V to 1 V at the transistor drain for each stage. Thus, the overall consumption of the circuit is approximately 13.5 mW. Layout simulations are done with Momentum Microwave. The layout was done in two main steps. Initially, electromagnetic simulations were

carried out in a partial way, i.e., by considering each element separately (p index). Then, in a second step, we simulated the whole structure of the LNA (g index). The results obtained then present differences related to the coupling phenomena between the different elements of the LNA, which are not taken into account in the partial simulations of these elements. These couplings result in a more or less pronounced degradation of the circuit's performance. In our case, we were able to distinguish the degradation of reflection coefficients both at the input S_{11} and output S_{22}. Since then, we have re-optimized the layout in order to minimize these degradations, but also to improve its gain and noise performance, see Figure 6 and Figure 7.
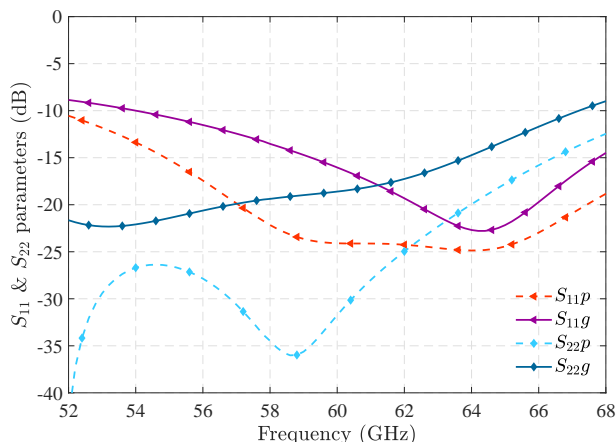

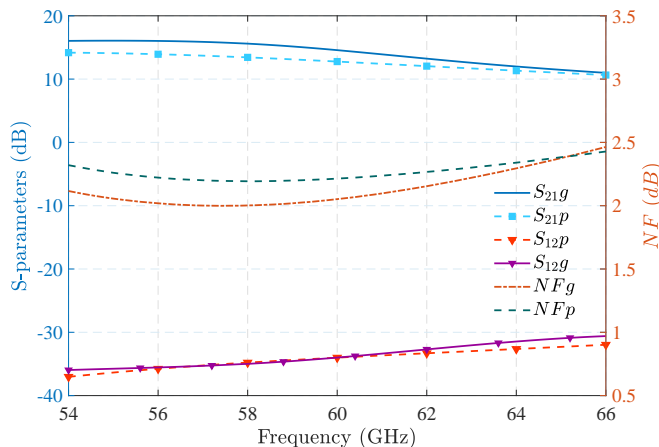Figure 6. S_{11} and S_{22} with partial and global layout simulations

Figure 7. S_{21}, S_{12} and NF with partial and global layout simulations

A final optimization of the layout was done to reduce the size of the circuit which was initially 1.29 x 1.56 mm^2. This allowed us to obtain the layout seen in Figure 5. The optimized LNA thus offers unconditional stability over a wide frequency range, see Figure 8. Post-layout simulations results are presented in Figure 9. There is a gain of 14.3 dB and a noise factor of 2.1 dB at 60.2 GHz. The reverse isolation is about -34 dB at 60.2 GHz and the reflection coefficients

S_{11} and S_{22} are less than -15 dB at 60.2 GHz. The 3 dB bandwidth (for $S_{11} < -10$ dB and $S_{22} < -10$ dB) ranges from 54 to 62.5 GHz with a fluctuation of about 0.17 dB in noise factor. The non-linear characteristics of the LNA are shown in Figure 10 and Figure 11. The simulated input 1 dB compression point of the LNA is $IP_{1dB} = -9.6$ dBm, while the input third order intercept point is $IIP3 = -4.8$ dBm.
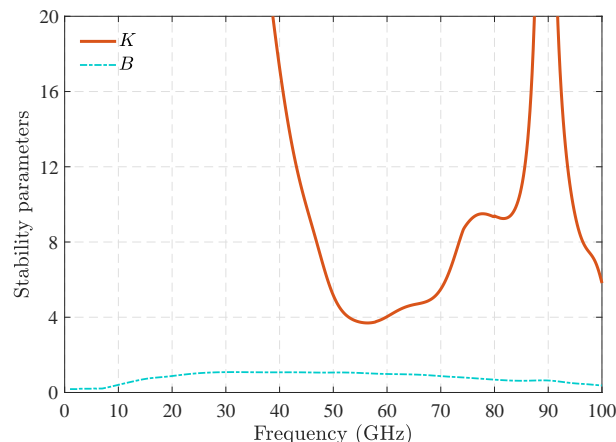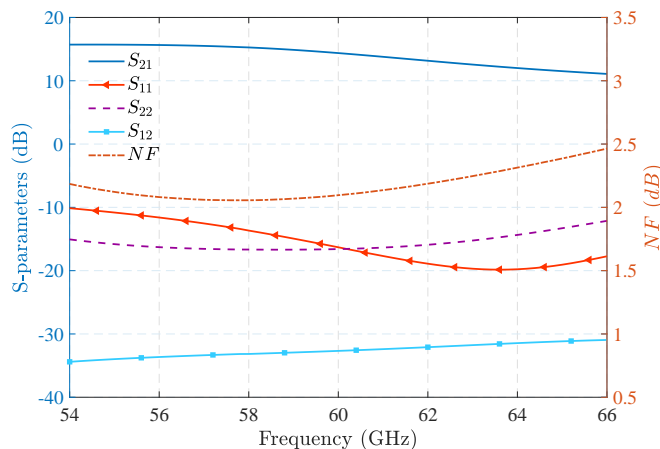

Figure 8. Stability parameters K and B

Figure 9. S-parameters and noise factor

The performance parameters of the designed LNA compared with other LNAs in the state-of-the-art are given in Table III. Our LNA shows good performance, especially in terms of noise factor, even if some of the results in the Table III are based on measurements. With a moderate power consumption compared to same type of technologies [4] [14] or even the 40 nm CMOS (Complementary Metal Oxide Semiconductor) [16], it presents a good gain to meet the targeted detection objectives. More gain can be achieved by increasing the drain voltage of the output stage or adding a fourth transistor. This would increase the power consumption and a little more the noise factor. The non-linear characteristics of the designed LNA are much better than those of the m-HEMT and CMOS technologies presented in Table III. For

TABLE III. PERFORMANCE COMPARISON

| Ref.	Technology	Freq. (GHz)	Gain (dB)	NF (dB)	IP_{1dB} (dBm)	IIP3 (dBm)	P_{DC} (mW)	Area (mm^2)
[2]	130 nm SiGe BiCMOS*	57-66	20.5	4.3	-17,8	-11,1	9.8	0.41 x 0.32
[4]	50 nm GaAs m-HEMT+	60-90	27	2.6	-26	-	45	1.6 x 2.3
[14]	100 nm GaAs m-HEMT+	60-90	19	2.5	-	-	56	3.5 x 1.0
[16]	40 nm CMOS+	60	12.5	3.8	-	-15	20.4	0.63 x 0.31
[17]	65 nm CMOS+	60	23	4	-26	-	8	0.35 x 0.14
[18]	90 nm CMOS+	58-77	11.2	4.8	-18.7	-7,4	10	0.72 x 0.76
[19]	65 nm CMOS+	60	20.2	5.2	-25	-	28	0.54 x 0.80
[20]	65 nm LP CMOS*	61	22	5.5	-	-10,7	26	0.71 x 0.46
This work	**70 nm GaAs m-HEMT***	**60**	**14.3**	**2.1**	**-9.6**	**-4.8**	**13.5**	**1.47 x 1.0**

+ Measures
∗ Simulations
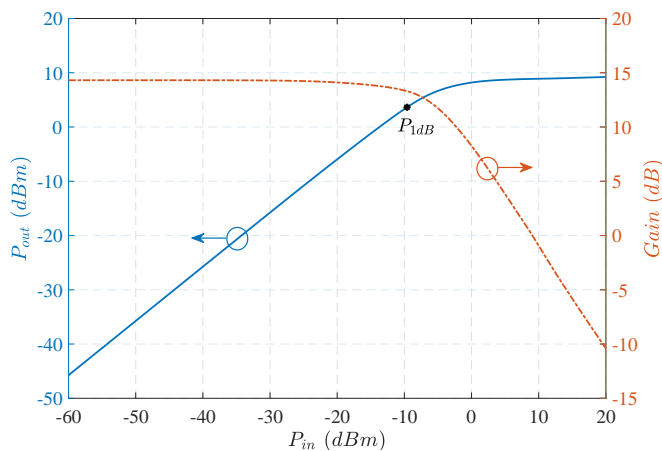
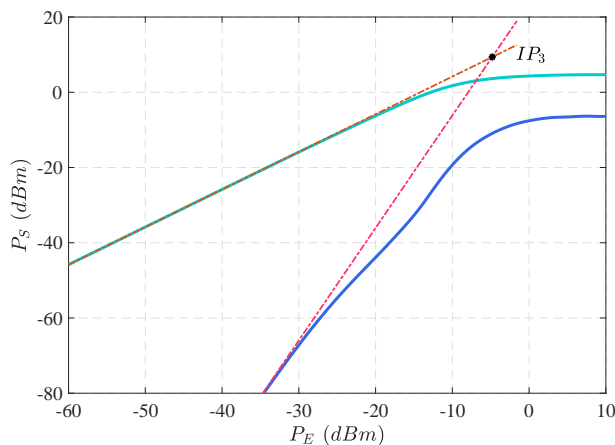Figure 10. Gain and 1 dB compression point

Figure 11. Three order intercept point (IP3)

example, its IP_{1dB} is -9.6 dBm, while it is less than -18 dBm for [4] [17]- [19]. It is the same for input three order intercept point ($IIP3$). The LNA occupies less space (1.47 x 1.0 mm^2) compared to the 50 and 100 nm GaAs m-HEMT technologies which occupy 2.3 x 1.6 mm^2 and 3.5 x 1.0 mm^2, respectively.

The performances thus obtained satisfy the specifications established in Table I, and allow, with the multi-band system, to detect up to 2.3 m the considered target (metallic cylinder of radius $r = 0.6$ cm and height $h = 5.4$ cm) at normal incidence, with a non-coherent integration. This represents an improvement of 30% in range compared to the conventional single-band detection system. In addition, by referring to [8], the overall detection coverage is also improved.

VII. CONCLUSION

A 60 GHz LNA designed in 70 nm GaAs m-HEMT technology was presented. The design was done with ADS Keysight in D007IH technology from OMMIC. Inductive degeneration of the source and inserting resistance in the bias circuit was used to better scale the transistor with a good trade-off between gain and noise, while ensuring unconditionnal stability. Our design was compared to other recently published milimeter-wave LNAs. Post-layout electromagnetic simulation results with momentum microwave show good performance, especially in terms of noise. With a noise factor of 2.1 dB at 60.2 GHz, our LNA is much better that those commonly found in the state-of-the-art. For a moderate power consumption of 13.5 mW, which is relativeley low for III-V's technologies, it presents 14.3 dB of gain at 60.2 GHz. The reflection coefficients of the designed LNA are less than -10 dB in 54-68 GHz. The input power at 1 dB compression point is $IP_{1dB} = -9.6$ dBm and the input third order intercept point is $IIP3 = -4.8$ dBm. The results of the designed LNA show the potential of III-V's technologies, especially the 70 nm GaAs m-HEMT for very low noise applications, particularly to improve the performance of detection systems.

REFERENCES

[1] A. C. Ulusoy et al., "A SiGe D-Band Low-Noise Amplifier Utilizing Gain-Boosting Technique," IEEE Microwave and Wireless Components Letters, vol. 25, no. 1, 2015, pp. 61–63.

[2] M. Pallesen, "Design of a 60 GHz Low Noise Amplifier in a 0.13 μm SiGe BiCMOS Process," Master's thesis, The University of Bergen, 2016, URL: http://bora.uib.no/handle/1956/12595 [accessed: 2017-10-24].

[3] A. Dyskin, D. Ritter, and I. Kallfass, "Ultra wideband cascaded low noise amplifier implemented in 100-nm GaAs metamorphic-HEMT technology," in Proceedings of the International Symposium on Signals, Systems, and Electronics (ISSSE) Oct. 3–5, 2012, Potsdam, Germany. IEEE, Dec. 2012, pp. 1–4.

[4] P. M. Smith et al., "A 50 nm MHEMT millimeter-wave MMIC LNA with wideband noise and gain performance," in Proceedings of the IEEE MTT-S International Microwave Symposium (IMS2014) June 1–6, 2014, Tampa, FL, USA. IEEE, Jul. 2014, pp. 1–4.

[5] Y. Chen et al., "OMMIC 70 nm mHEMT LNA design," in Proceedings of the IEEE Asia Pacific Microwave Conference (APMC) Nov. 13–16, 2014, Kuala Lumpar, Malaysia. IEEE, Jan. 2018, pp. 1192–1195.

[6] D. K. Barton, Frequency Diversity Theory. Artech House Inc., 1977, vol. 6 of Radars, section 2, pp. 35–114, in Frequency Agility and Diversity, ISBN: 0-89006-067-3.

[7] P. S. Diao, T. Alves, B. Poussot, and M. Villegas, "A new method and transceiver architecture dedicated to continuous detection of very small metallic object," in Proceedings of the 10th Global Symposium on Millimeter-Waves (GSMM) May 24–26, 2017, Hong Kong, China. IEEE, Jul. 2017, pp. 169–171.

[8] P. S. Diao, T. Alves, M. Villegas, and B. Poussot, "Compact millimeter wave architecture dedicated to object detection using dual band-dual polarization and impulse method," in Proceedings of the 13th Conference on Ph.D. Research in Microelectronics and Electronics (PRIME) June 12–15, 2017, Giardini Naxos, Italy. IEEE, Jul. 2017, pp. 161–164.

[9] P. Surendran, J.-H. Lee, and S. J. Ko, Performance of Non-coherent Detectors for Ultra Wide Band Short Range Radar in Automobile Applications. Springer-Verlag Berlin Heidelberg, 2012, vol. 377, pp. 185–195 in Software Engineering Research, Management and Applications 2011, ISBN: 978-3-642-23201-5.

[10] M. I. Skolnik, The Radar Equation, 2nd ed. McGraw Hill, Inc., 1980, chapter 2, pp. 15–67, in Introduction to Radar Systems, ISBN: 0-07-057909-1.

[11] R. Abdaoui, M. Villegas, G. Baudoin, and A. Diet, "Microstrip band pass filter bank for 60 GHz UWB impulse radio multi band architectures," in Proceedings of the IEEE MTT-S International Microwave Workshop Series on Millimeter Wave Integration Technologies Sept. 15–16, 2011, Sitges, Spain. IEEE, Oct. 2011, pp. 192–195.

[12] "SG13S Process Specification Rev. 1.06," July 2016, URL: https://www.ihp-microelectronics.com/en/services/mpw-prototyping/sigec-bicmos-technologies.html [accessed: 2017-10-18].

[13] "D007IH Design Manual - OM-CI/008/MG," Oct. 2017, URL: http://www.ommic.fr/site/mpw-4r [accessed: 2018-07-20].

[14] A. Bessemoulin, J. Grunenputt, P. Felton, A. Tessmann, and E. Kohn, "Coplanar W-band low noise amplifier MMIC using 100-nm gate-length GaAs PHEMTs," in Proceedings of the 34th European Microwave Conference Oct. 12–14, 2004, Amsterdam, The Netherlands, vol. 1. IEEE, 2005, pp. 25–28.

[15] S. P. Voinigescu et al., "A scalable high-frequency noise model for bipolar transistors with application to optimal transistor sizing for low-noise amplifier design," IEEE Journal of Solid-State Circuits, vol. 32, no. 9, 1997, pp. 1430–1439.

[16] H. Gao et al., "A 4861 GHz LNA in 40-nm CMOS with 3.6 dB minimum NF employing a metal slotting method," in Proceedings of the IEEE Radio Frequency Integrated Circuits Symposium (RFIC) May 22–24, 2016, San Francisco, CA, USA. IEEE, Jul. 2016, pp. 154–157.

[17] E. Cohen, O. Degani, and D. Ritter, "A wideband gain-boosting 8 mW LNA with 23 dB gain and 4 dB NF in 65 nm CMOS process for 60 GHz applications," in Proceedings of the IEEE Radio Frequency Integrated Circuits Symposium June 17–19, 2012, Montreal, QC, Canada. IEEE, Jul. 2012, pp. 207–210.

[18] Y.-S. Lin, C.-Y. Lee, and C.-C. Chen, "A 9.99 mW low-noise amplifier for 60 GHz WPAN system and 77 GHz automobile radar system in 90 nm CMOS," in Proceedings of the IEEE Radio and Wireless Symposium (RWS) Jan. 25–28, 2015, San Diego, CA, USA. IEEE, 2015, pp. 65–67.

[19] C. So and S. Hong, "60 GHz variable gain LNA with small NF variation," in Proceedings of the IEEE International Symposium on Radio-Frequency Integration Technology (RFIT) 30 Aug.–1 Sept., 2017, Seoul, South Korea. IEEE, Sep. 2017, pp. 171–173.

[20] A. Wang, L. Li, and T. Cui, "A transformer neutralization based 60 GHz LNA in 65 nm LP CMOS with 22 dB gain and 5.5 dB NF," in Proceedings of the IEEE International Symposium on Circuits and Systems (ISCAS2013) May 19–23, 2013, Beijing, China. IEEE, Aug. 2012, pp. 1111–1114.